

Optimization-based Modeling and Analysis of Brine Reflux Osmotically Assisted Reverse Osmosis for Application toward Zero Liquid Discharge Systems

Elmira Mohammadi Shamlou¹, Radisav Vidic^{1,2}, Mahmoud M. El-Halwagi³, and Vikas Khanna^{1,2*}

¹ Department of Civil and Environmental Engineering, University of Pittsburgh, 3700 O'Hara Street, 742 Benedum Hall, Pittsburgh, Pennsylvania 15261, United States

² Department of Chemical and Petroleum Engineering, University of Pittsburgh, 3700 O'Hara Street, 742 Benedum Hall, Pittsburgh, Pennsylvania 15261, United States

³ Department of Chemical Engineering, Texas A&M University, 3122 TAMU, 100 Spence St., College Station, TX 77843

*Address correspondence to khannav@pitt.edu

Abstract

Significant amounts of high-salinity wastewater generated by water-intensive industrial activities such as shale oil and gas production have raised serious environmental concerns in recent years. Existing and emerging desalination technologies offer promise to manage these high salinity wastewater streams while simultaneously producing fresh water that could be diverted for beneficial uses. Osmotically assisted reverse osmosis (OARO) is one such emerging desalination technology capable of handling hypersaline brines and achieving high recoveries. However, rigorous modeling and analysis is needed to evaluate the process performance, energy consumption, and treatment cost of various OARO configurations. This work presents detailed modeling and analysis of brine-reflux OARO (BR-OARO) system and compares it with other

commonly discussed configurations, including cascading osmotically mediated reverse osmosis (COMRO), consecutive loop OARO, and split feed counterflow RO, through a cost optimization-based framework. We analyze and compare the treatment costs, membrane area, specific energy consumption, and design parameters of the aforementioned configurations with the ultimate goal of achieving zero liquid discharge (ZLD). The results indicate that the BR-OARO system with treatment cost of 5.1 US \$/m³ of produced water with 10% salinity outperforms other configurations in terms of number of stages needed, treatment cost, membrane area, and energy consumption.

Keywords: Osmotically assisted reverse osmosis, brine reflux OARO, consecutive loops OARO, split feed OARO, COMRO, shale gas produced water

Introduction

The growth of water-intensive industries and the wastewater they generate have all contributed to rising environmental concerns around both water quality and quantity. Processes such as shale oil and gas production, flue gas desulfurization, and brackish water desalination generate large amounts of brine, which can have detrimental impacts on the environment if not properly managed [1-8]. Given fresh water scarcity, tightening environmental regulations, and the high cost of brine disposal, hypersaline brine streams could provide a win-win opportunity for recovering clean water as well as minimizing the volume of wastewater to be managed via disposal. This can also alleviate stress on freshwater resources and mitigates adverse environmental impacts. As such, Zero Liquid Discharge (ZLD) solutions that reduce waste to solids while increasing water recovery, are gaining traction in academia as well as industry [9, 10]. The ZLD process entails concentrating water to its saturation salinity limit and then passing

it through a crystallizer. Thermal distillation is a common desalination method used to treat hypersaline brines to achieve water recovery up to the point of saturation. However, in general, evaporative-based technologies are inefficient in terms of energy consumption due to the phase change involved, which consumes far more energy than the minimum work of separation [11-13].

Having higher energy efficiency in comparison to thermally driven desalination processes, reverse osmosis (RO) is the most widespread technology accounting for 69% of the desalination capacity worldwide [14, 15]. RO is a pressure driven separation process utilizing hydraulic pressure to force the solvent (water) to move through a semipermeable membrane from higher solute concentration to lower concentration. The required permeate recovery, or desired concentrate salinity determines the energy required for separation process. The minimum applied hydraulic pressure in RO process should be at least as high as the terminal osmotic pressure difference (at the most concentrated state of the feed solution) so that permeation occurs across the entire available membrane area [16]. This implies that higher recovery ratios, or higher feed salinities increase the required applied hydraulic pressure, impacting the economic feasibility of the process by increasing both capital and operating costs. In addition, the applied hydraulic pressure is limited by the maximum pressure that RO membranes and membrane modules can withstand.

Multi-stage RO (MSRO) systems have been suggested to decrease the required energy of separation through stagewise increase in the terminal pressure difference [17]. The energy savings in this configuration arise from operating the system at higher feed flowrates with lower terminal pressure difference corresponding to lower brine salinities at initial stages, and reduced feed flowrate with higher terminal pressure difference in latter stages [16, 18, 19]. Although

MSRO configuration could result in energy savings, the problem of maximum allowable pressure for RO membranes still remains an issue for high permeate recoveries and high feed salinities, such as those encountered in high salinity wastewater from shale oil and gas operations [20].

Osmotically assisted reverse osmosis (OARO) systems are emerging RO configurations that enable the pressure driven membranes to treat hypersaline solutions [21, 22]. OARO overcomes the problem of excessive hydraulic pressures by introducing a saline solution stream on the low-pressure side of the membrane leading to reduction in transmembrane osmotic pressure difference [21, 23-25]. Permeate donating saline stream is concentrated on the high-pressure side of the membrane, while permeate receiving saline stream is diluted on the low-pressure side of the membrane. This process is also referred to as countercurrent flow reverse osmosis (CFRO) given the fact that the concentrating and diluting saline solution flow (move) in the opposite direction. In this countercurrent flow mode, the concentration of both concentrating and diluting saline solution increase in the concentrating flow direction along the module which minimizes the local osmotic pressure difference and increases the system's second law efficiency by creating a balanced driving force throughout the module[26, 27]. OARO systems mainly produce concentrate of high salinity and cannot produce pure water on its own. Therefore, OARO is usually coupled with an RO process for freshwater production [28].

Various OARO configurations have been proposed in the available literature. The key difference among various OARO systems is the source of saline diluting solution stream on the low-pressure side of the OARO unit, which could be: 1) working solution, 2) concentrate, and 3) feed stream. Depending on the plant makeup feed salinity and the configuration selection, plant makeup feed may enter the system as: 1) diluting stream of the OARO unit, 2) feed stream of the

RO unit, and 3) concentrating feed of the OARO unit. Both OARO and RO systems can be configured in multi-stage operation mode to increase water recovery and improve energy efficiency.

The most frequently discussed OARO configurations in the literature are consecutive loop osmotically assisted RO (CL-OARO) [29, 30], split feed counterflow RO (SF-OARO) [27], and cascading osmotically mediated RO (COMRO) [20], the details of which will be discussed in the following sections. To achieve high recoveries, CL-OARO and SF-OARO require multiple stages, which adds to their design complexity. On the other hand, regardless of number of stages, recovery is extremely limited for the COMRO configuration which was developed based on the same premise as MSRO (i.e. energy savings through stagewise increases in terminal pressure difference).

In this work, we present the rarely discussed brine reflux osmotically assisted RO (BR-OARO) configuration, which, in contrast to CL-OARO and SF-OARO, is capable of achieving high recoveries without the use of multiple stages. Similar to COMRO, BR-OARO can be configured in multiple stages for energy savings. The concept of brine reflux reverse osmosis was first introduced in 1973 by Loeb and Bloch [28]. In this study, a salinity-dependent feed entrance option is incorporated into an optimization-based design for BR-OARO. We developed mathematical models of the BR-OARO, COMRO, SF-OARO, and CL-OARO configurations at the module scale and compared their maximum achievable recovery, energy consumption, cost, and membrane requirement using an optimization-based framework. Furthermore, we investigated the underlying cause behind the CL-OARO and SF-OARO low recoveries at lower number of stages. In addition, we investigated whether cascading stages in series (as in COMRO and BR-OARO) save energy in OARO systems in a similar manner to MSRO systems. Finally,

we conclude the manuscript with a sensitivity analysis of the feed salinity and burst pressure of the membrane on the overall treatment cost.

Methodology

Process description

COMRO- The COMRO configuration is illustrated in Figure 1a). It consists of an initial RO stage followed by multiple stages of OARO modules connected in series. The plant feed enters the system through the inlet of the last OARO stage's diluting stream channel. Except for the first OARO stage, the diluting stream exiting each OARO stage enters the preceding stage's diluting stream channel. However, the diluting stream that exits the first OARO stage enters the RO stage as a concentrating stream. The reject stream from the RO stage is directed into the first OARO stage as a concentrating stream. Similarly, the concentrating stream exiting each OARO stage enters the following OARO stage for further concentration, and the plant reject stream exits the system at the final OARO stage. This configuration makes use of two energy recovery devices (ERDs). One is used to recuperate the energy contained in the RO reject stream and pressurize the RO inlet stream. The level of depressurization and pressure of the stream entering the first OARO concentrating channel will be determined through optimization. The second ERD device is assigned to recover energy from the system's reject brine and to pressurize the concentrating stream entering the first OARO stage. The model developed in this study is based on the assumption that the reject brine is completely depressurized.

As discussed by Bouma [27], one issue with the COMRO configuration is the imbalance of the system flowrates on the concentrating and diluting sides. The flowrate of the dilute stream is highest at the diluting outlet of the first OARO stage (entrance of the RO stage) in COMRO. In comparison, the flowrate of the inlet of the concentrating stream of the first OARO stage

(corresponding to RO outlet) is significantly lower due to dewatering in the RO stage. Because of the flowrate imbalance, changes in salinity on the concentrating side are greater than those on the diluting side, resulting in an osmotic pressure difference imbalance throughout the system.

Brine Reflux (BR)- OARO- The BR-OARO configuration is depicted in Figure 1b). As with COMRO, it consists of an initial RO stage followed by a train of OARO stages, with each stage's reject concentrate serving as the concentrating stream for the subsequent stage. A portion of the concentrate reject brine exiting the final OARO stage is recycled into the final stage's diluting channel as a diluting stream. The diluting stream with the lowest salinity exits the first OARO stage and is used as feed in the RO stage to produce high purity permeate. Feed can enter the process at multiple locations in this configuration, including the inlet or outlet of the RO or any OARO stages. The ERD devices operate similarly to those described in the COMRO configuration.

Although the BR-OARO configuration appears to be similar to the COMRO configuration, we will demonstrate that the imbalance problem associated with COMRO does not exist for BR-OARO due to the presence of the recirculating stream and the ability to choose optimum feed entrance location (elaborated further in the stage flowrate and salinity sub-section under “Results and Discussion” section).

Consecutive loop (CL)- OARO- The CL-OARO configuration depicted in Figure 1c) employs a sweep solution as a diluting agent that may or may not contain the same constituents as the plant feed. This enables this configuration to benefit from using thermo-responsive draw solution as sweep solution, similar to forward osmosis [31]. However, for the purposes of comparison across configurations, the sweep stream in CL-OARO is assumed to be a non-responsive solution containing the same constituent as plant feed. The plant feed enters the final

OARO stage's concentrating stream channel, and the reject brine exits the system through the same final stage. The diluting stream exiting each OARO stage serves as the concentrating stream for the preceding stage. As a result, the first OARO stage's diluting stream serves as the concentrating stream of the first RO stage, where fresh water is produced. Due to the membranes' imperfect salt rejection, a portion of the concentrating stream at the outlet of the concentrating channel of each stage is recycled to the inlet of the diluting side of the second subsequent stage. This maintains steady state operation and prevents salt buildup in one loop. The recycle stream from the final stage is purged. Since the concentrating stream exiting each stage serves as the diluting stream for the following stage, it is completely depressurized, and its energy is recovered by the concentrating stream entering the same stage.

Split-Feed (SF) OARO- Figure 1d) depicts the SF-OARO configuration. Each stage's concentrating and diluting solution is sourced by a mixture of reject brine from the previous stage and diluted solution exiting the subsequent stage. This mixture is split by a ratio (referred to as split feed ratio in this study) between the sides of each stage. The split feed ratio is calculated by dividing the flowrate of the mixture entering the concentrating side by the total flowrate of the mixture. The dilute solution that exits the first OARO stage flows into the RO stage for freshwater recovery, while the RO reject flows to the OARO stages for further concentration. The final OARO stage's concentrate stream exits the system as reject brine. As with the BR-OARO system, feed can enter the SF-OARO system at a variety of locations, including the RO or OARO stages' inlet and outlet. Each stage has one ERD device assigned to recover energy from the exiting concentrating stream and pressurize the stage's entering concentrating stream

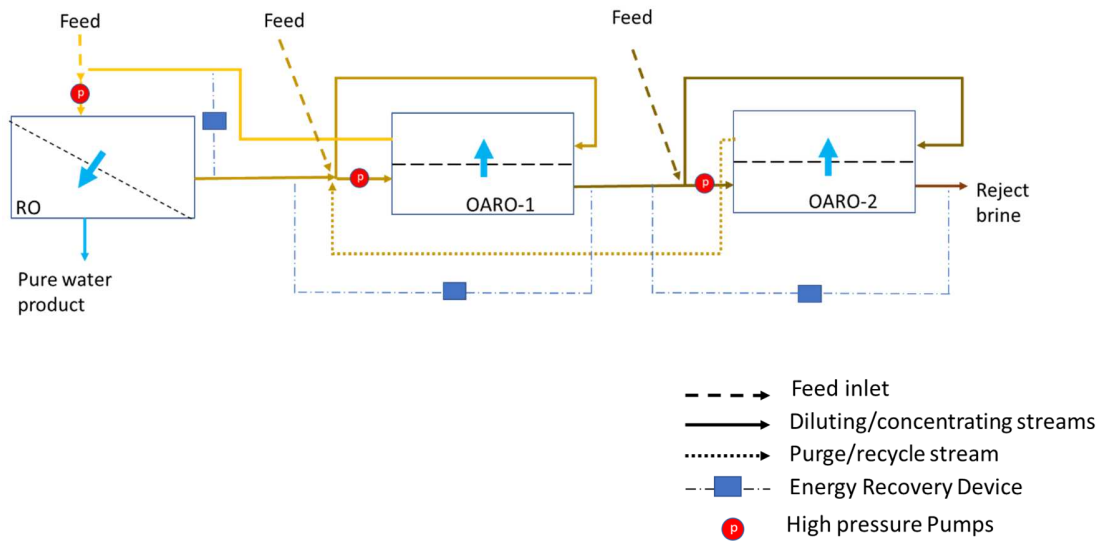


Figure 1. OARO configurations: a) Cascading osmotically mediated RO b) Brine reflux-OARO, c) Consecutive loops-OARO, d) Split feed-OARO. Different configurations are depicted using just two OARO stages and do not include low pressure or booster pumps for the sake of simplicity.

High pressure, booster, and low pressure pumps- A high pressure pump is located prior to the inlet of each stage's concentrating channel to provide the energy required for separation. It should be noted that each membrane stage's length and width are comprised of multiple membrane modules connected in series or parallel. If only one high pressure pump is added prior to each stage's concentrating inlet, the pressure drop across the stage will obstruct the optimal separation process by reducing the flux. Additionally, the maximum pressure at the inlet of each stage is limited by the burst pressure of the membranes. Booster pumps are therefore added between the concentrating sides of each stage's modules to maintain the required pressure for the separation process throughout the stage.

Low pressure pumps are used to provide the energy required for the stream to flow in the diluting channels while retaining the diluting stream pressure low enough in comparison to the concentrating side to maintain optimal separation driving force. If only one pump is added prior

to each stage's diluting inlet, there is a need to pressurize the diluting solution to a high level comparable to the pressure provided by the concentrating side's high-pressure pump to compensate for the pressure drop in long stages. This reduces the driving force and flux throughout the stage. As a result, installing multiple low pressure pumps between the modules of a stage is preferable and compensates for the pressure drop. The appendix section contains additional information for modeling the pumps.

Choice of membrane- The operation of salinity gradient membrane-based separation processes is affected by concentration polarization (CP). CP occurs when the solute concentration increases near the membrane surfaces at the boundary layer of the concentrating channel and decreases near the membrane surfaces at the boundary and support layers of the diluting channel. This reduces the driving force of separation by increasing the osmotic pressure gradient across the membrane. For RO membranes with pure water on the permeate side, CP occurs only on the feed concentrating side. However, CP occurs on both sides in OARO processes with saline solution on the concentrating and diluting sides. Specifically, the presence of a support layer on the dilute side intensifies CP, impeding the separation process further. The CP is affected by the support layer structural parameter that is directly correlated to the thickness and tortuosity and is inversely correlated to the porosity of the support layer. Reduced structural parameters improve permeate and diluting solution mixing, resulting in less concentration polarization. However, membranes with a lower structural parameter (for example, forward osmosis (FO) and pressure retarded osmosis (PRO) membranes) have a lower strength and burst pressure, typically less than 24 bar [32-35], which limits the applied hydraulic pressure for the separation process. Straub et al. [36] conducted a study in which the burst pressure of the pressure retarded osmosis (PRO) membrane was boosted to around 50 bar using feed spacers.

We have used the same membrane characteristic and burst pressure as in [36] as an optimistic yet feasible choice for OARO membranes given current advances in membrane technology. The maximum burst pressure for the initial RO stage is assumed to be 85 bar, which is typical for seawater desalination reverse osmosis (SWRO) membranes. The characteristics of both RO and OARO membranes are listed in Table A.2.

Modeling OARO process- Individual OARO stages operate identically in all OARO configurations; the primary differences arise from the source of diluting and concentrating solution and the manner in which OARO stages are connected to one another. Each OARO stage is composed of a series/or parallel arrangement of OARO modules, the combination of which determines the stage's total width, length, and area.

We developed detailed mathematical models for the four OARO configurations shown in Figure 1 and described above. To model the large-scale modules, we used a discretization method in which each stage of the RO and OARO modules is divided lengthwise and mass and energy balances are calculated for each slice (Figure A.7). The common equations used to model the process are discussed here, and the detailed equations and correlations for each configuration are listed in tables A.6 to A.10.

The membranes used in this study are not ideal in terms of salt rejection, and there is salt flux through the membrane in addition to water flux. As a result, the total mass flux passing through each membrane slice is equal to the sum of salt and water fluxes (Equation 1).

$$j_{\text{total}}^{i,z} = j_w^{i,z} \rho_w^{i,z} + j_s^{i,z}$$

(1)

The water flux is determined by the water permeability coefficient and the difference in hydraulic and osmotic pressures across the membrane. (Equation 2).

$$J_w^{i,z} = a_w (P_c^{i,z} - P_d^{i,z} - OP_{c_m}^{i,z} + OP_{d_m}^{i,z})$$

(2)

The osmotic pressure is proportional to the salinity and temperature of the stream via the osmotic coefficient (Equation 3).

$$OP_{c_m}^{i,z} = \frac{vRT}{M_w} C\alpha \quad (3)$$

Salt flux through the membrane is a function of salinity gradient across the membrane and is calculated using the membrane salt permeability coefficient (equation 4).

$$J_s^{i,z} = a_s (C_{c_m}^{i,z} - C_{d_m}^{i,z})$$

(4)

The change in flowrate across each membrane slice is the product of the area and total mass flux received or donated for diluting and concentrating solution, respectively (Equations 5 and 6).

$$M_{C_{out}}^{i,z} = M_{C_{in}}^{i,z} - (J_w^{i,z} \times \rho_w + J_s^{i,z}) L^{i,z} W^i$$

(5)

$$M_{d_{in}}^{i,z} = M_{d_{out}}^{i,z} - (J_w^{i,z} \times \rho_w + J_s^{i,z}) L^{i,z} W^i$$

(6)

The pressure drop per unit of membrane length is equal to the change in hydraulic pressure across each slice of the membrane for both diluting and concentrating streams (Equation 7):

$$P_{C/d_{in}}^{i,z} - P_{C/d_{out}}^{i,z} = PD_{c/d}^{i,z} L^{i,z}$$

(7)

The remaining model consists of equations that describe the connection between slices of the RO or OARO modules, equations that describe the connection between the stages specific to each type of OARO configuration, as well as inclusion of high-pressure pumps, low

pressure/booster pumps, and energy recovery devices based on their location in the system. Appendix Tables A6 to A10 provide equations and correlations used to model each configuration.

Optimization model- We developed non-linear optimization models for each of the studied OARO configurations using the mathematical models developed for each configuration and representative cost equations for capital (membrane, pumps, and ERD devices) and operating costs (electricity, membrane replacement, pretreatment, labor, and maintenance). The stream's pressure, salinity, and flowrate are independent variables, while the dimensions of each stage, the size of the pumps, and the ERD devices are dependent variables. The non-linear programming models are implemented in GAMS software and solved with the CONOPT4 solver [37]. We ran the optimization model of each configuration for two sets of optimization objectives: 1) the maximum amount of water that each configuration can recover under specified conditions,

$$\max WR(y), y = (P, M, X)^T \in \mathbb{R}$$

$$\text{s. t. } \varphi(y) = 0$$

$$\psi(y) \leq 0$$

and 2) the minimum cost associated with achieving a certain specified level of water recovery corresponding to the reject brine's saturation salinity (or ZLD condition) for each configuration:

$$\min TUC(y), y = (P, M, X)^T \in \mathbb{R}$$

$$\text{s. t. } \varphi(y) = 0$$

$$\psi(y) \leq 0$$

$$WR = WR_{ZLD}$$

The stage count is specified as a known parameter in the optimization model, and the effect of changing the stage count on the results is investigated by running scenarios of the optimization model with different stage counts.

Results and discussion

We performed two sets of optimizations for a hypothetical OARO plant treating 10 kg/s produced water with 10% (wt/wt) salinity with OARO membrane burst pressure of 50 bar. Tables A.2 to A.4. in the appendix provide the model input parameters, including plant characteristics, membrane properties, and capital and operating cost data.

Maximum recovery- Figure 2 depicts the maximum achievable recovery versus the number of stages for two pressure levels of 20 and 50 bar for a 10% feed salinity. The stage count excludes the initial RO stage and only includes OARO stages. For a 10% feed salinity, 74% water recovery corresponds to the reject brine's saturation salinity or ZLD condition (as shown by the yellow line in Figure 2.). The BR configuration outperforms the COMRO, CL and SF configurations by achieving ZLD conditions at a pressure as low as 20 bar and with only one OARO stage. The maximum water recovery of the CL and SF configurations increases with an increase in the number of stages, and both configurations require a larger number of stages to achieve conditions for ZLD recovery at lower pressure levels. Water recovery in the COMRO configuration is independent of the number of stages (i.e. increasing the number of stages does not improve recovery) and only varies with applied hydraulic pressure. For example, at the applied hydraulic pressure of 20 and 50 bar, COMRO has water recovery of 16% and 33%, respectively, which is significantly less than ZLD conditions.

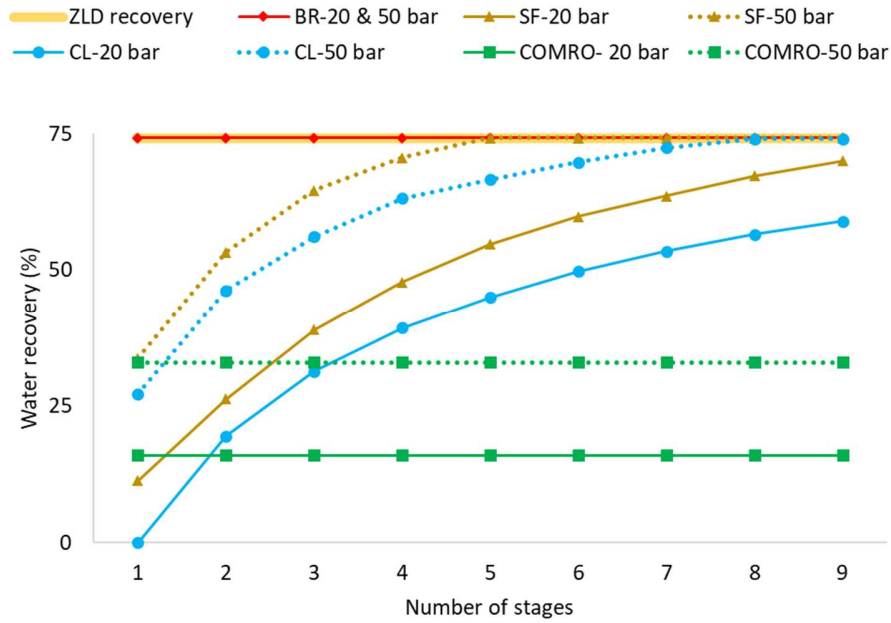


Figure 2. Maximum possible recovery vs. number of stages for OARO systems at pressure levels of 20 and 50 bar. The feed salinity is fixed at 10% (wt/wt). The maximum pressure in the RO stage is assumed to be 85 bar.

In a single stage OARO, the maximum water recovery or maximum reject brine salinity is achieved when the terminal hydraulic pressure difference equalizes the terminal osmotic pressure difference at the stage's exit (i.e., where the diluting solution enters and the concentrating solution exits). The terminal osmotic pressure difference is determined by the diluting stream inlet salinity and concentrating stream outlet salinity. For a given applied pressure, the higher the recovery, the higher the diluting concentration required at the OARO stage's exit. The BR-OARO configuration can achieve ZLD recovery with only one OARO stage because the diluting stream (or recycle stream) inlet concentration is as high as reject brine at saturation.

The primary reason that SF and CL configurations require multiple OARO stages to achieve high level of recovery is that a single stage SF and CL configuration imposes salinity limitation on the stream at the inlet of the diluting channel. As shown in Figure 2, single stage CL and SF configurations can only achieve 27% and 33% recovery, respectively at 50 bar applied hydraulic pressure. In a single stage CL configuration, the diluting side's inlet salinity is constrained by the RO outlet salinity, thereby constricting the terminal osmotic pressure difference, recovery, and concentrate stream outlet salinity. In multiple stage CL, the increase in recovery with each additional stage is limited because each stage's diluting solution inlet salinity is equal to the concentrate stream outlet salinity of the preceding stage, which is limited by the preceding stage's diluting solution inlet salinity. As a result, the restriction imposed by the RO stage's outlet salinity (dilute side inlet to first CL stage) propagates throughout the subsequent OARO stages, requiring the system to operate at a high number of stages to achieve the desired level of recovery.

Likewise, recovery in a single stage SF configuration is constrained by the salinity of the RO reject (and feed salinity if the feed is introduced after the RO stage) because the diluting and concentrating streams have the same inlet salinity as the previous stage's reject stream. To maximize recovery, multiple split feed stages should be connected together, each with a recovery limitation imposed by the stage feed salinity. The same rationale explains COMRO's limited recovery, which cannot be increased by adding OARO stages. Regardless of the number of stages in COMRO, the final stage's dilute inlet salinity is always equal to the plant feed salinity, thereby limiting the amount of osmotic assistance that is required for high water recoveries. Rather than dealing with the complexities and limitations of the CL and SF configurations, we can simply recirculate the brine as in the BR configuration to achieve high recovery in just one

stage or multiple stages in series. In the following sections, the performance of the BR, CL, and SF configurations will be discussed in greater depth. COMRO is excluded from further analysis because the achievable water recovery is extremely limited at the study's maximum burst pressure of 50 bar.

Selection of feed location for BR and SF- We investigated the effect of feed inlet location on treatment cost in single stage BR and SF configurations since these two configurations allow for multiple feed inlets (Figure A1). We conducted the analysis for two salinity levels: 3.5% and 10% (this salinity level is also close to the maximum salinity that RO reject can achieve at 85 bar burst pressure) to determine the optimal feed inlet location based on salinity. We compared two potential feed entrance locations: RO inlet and RO outlet. Our findings show that for both BR and SF, the lowest cost is obtained when the feed enters the system at the RO outlet for 10% salinity feed, while the lowest cost is obtained when the feed enters the system at the RO inlet for 3.5% salinity feed. Such finding can be explained by the fact that if the high salinity feed enters the system at the RO inlet, it either raises the RO inlet salinity or increases the volume of recirculated diluting solution from the subsequent OARO stage to keep the RO inlet salinity low. Both of these phenomena increase the system's energy consumption. Similarly, introducing a low salinity feed at the RO outlet dilutes the concentrated stream, thereby increasing the energy and membrane area required for reconcentration. Our subsequent modeling and analysis assumed that the feed (10% salinity) enters the SF and BR systems at the RO outlet prior to the first OARO stage.

Treatment cost. The variation in treatment costs as a function of the number of stages is depicted in Figure 3a. The analysis of SF and CL configurations begins at 6 and 8 stages,

respectively, as this is the minimum number of stages required to achieve water recovery corresponding to saturation salinity (i.e., ZLD conditions). For the BR configuration, increasing the number of stages up to three results in a cost savings of approximately 10%, after which the cost savings become very marginal. For the SF configuration, increasing the number of stages initially results in a significant cost reduction of around 47% and then starts showing diminishing returns after ten stages. Even with a large number of stages (larger than 20), both BR and SF configurations do not achieve the absolute minimum cost; however, after a certain number of stages (3 for BR and 10 for SF), the reduction in treatment cost becomes negligible (less than 2 percent). The treatment cost for CL is minimum at nine stages, one stage more than the minimum number of stages required for ZLD, and increasing the number of stages further increases the treatment cost. As a result, the optimal number of stages for BR, SF, and CL configurations are 3, 10, and 9 stages, with treatment costs of 5.1, 5.9, and 7.22 $\$/\text{m}^3_{\text{feed}}$, respectively. This demonstrates that BR outperforms two other configurations in terms of cost and stage count.

The cost breakdown analysis in Table A1 demonstrates that membrane capital and replacement costs, as well as electricity costs, account for the majority of the cost and are the primary reason for the difference in treatment cost between different configurations. Next, we describe the underlying reason for energy and cost savings associated with multiple OARO stages.

Total specific energy consumption- Figure 3b illustrates the change in specific energy consumption (SEC) for the three OARO configurations as the number of stages increases. All configurations have similar SEC at their smallest number of stages (1, 6, and 8 for BR, SF, and CL, respectively), which decreases for BR and SF configurations as the number of stages increases. In the CL configuration, however, SEC rises as the number of stages increases. The

reduction in SEC of BR and SF with increasing number of stages is directly influenced by the Reynolds number (Re) lower bound (minimum allowable Reynolds number) in the model. When designing and analyzing an OARO plant, boundaries on Reynolds number are established to ensure practical design. We set the lower and upper bounds of Re to 100 and 2000 [30], respectively. While higher Re values promote mixing and decrease CP, resulting in increased flux and decreased membrane area, they also increase the pressure drop in the module. Despite the effect of Re on CP, our analysis shows that the cost-optimal design for OARO modules tends to reduce Re at the diluting stream inlet of each stage to the lowest possible Re value (Re of 100). This is because OARO membranes, regardless of their Re value, operate over large areas with low fluxes. As a result, the small reduction in membrane area and associated cost at higher Re is heavily outweighed by the increased electricity cost due to the large pressure drop across large membrane areas. As a result, the best system design is one that operates at low Re numbers.

The flowrates of both diluting and concentrating streams in OARO stages reduce along the stage in the same direction with concentrating stream flow. Therefore, in a single OARO stage, where the width is identical throughout the module, terminal point of the stage has the lowest flowrate with lowest allowable Re. As such, in case of single stage OARO, initial part of the stage with high flowrate has high Re number and high pressure drop which result in high SEC. This issue could be addressed in two ways: 1) by relaxing the lower bound on Re, which enables the stage width to increase to reduce the pressure drop in the initial part of the stage 2) by designing the system in multiple stages, where staging provides the opportunity to change the width along the concentrating flow direction. With constant Re number lower bound, initial stages with higher flowrate can have higher width and lower Re number and pressure drop

resulting in energy saving. Our analysis for BR-OARO configuration shows that as the Re number increases, higher number of stages are required to prevent the pressure drop.

While SEC of BR and SF configurations decreases with an increase in the number of stages, this is not the case for CL configuration. Because the stages in CL are not connected in series, the flowrate change occurs in each stage independently. Therefore, each stage of CL acts like a single stage BR and adding additional looping stages does not reduce the SEC. Instead, it increases the SEC due to additional need for pressurization and circulation. The results in Figure 3b reveal that the SEC of CL with 9 stages is equal to the SEC of a single stage BR. To improve the overall SEC for CL configuration, each stage should be subdivided into multiple stages in series, which adds to design and operation complexity. The results in Figure 3b show that BR, SF, CF have SEC of 12.1, 13.1, and 20 kWh/m³_{feed} at their cost optimum number of stages, which shows that BR is superior to other OARO configurations in terms of energy consumption.

Total membrane area- Figure 3c shows the variation in total membrane area as a function of number of stages. For BR, the area changes very marginally as the number of stages increases. The reduction in treatment cost for BR configuration with increasing number of stages is primarily attributable to the reduction in SEC with practically no observable change in capital cost. For CL and SF configurations, increasing the number of stages from the minimum to the optimal number reduces the total membrane area by 50% and 15%, respectively because CF and SF rely on stagewise increases in both concentrating stream outlet salinity and diluting stream inlet salinity to achieve a specific reject brine salinity at the final stage. Given a constant plant feed and final reject brine salinity, reducing the number of stages increases the terminal

concentration difference (i.e. concentration difference between the concentrate outlet and dilute inlet of each stage) and thereby reduces the average driving force and flux leading to an increase in required membrane area, which increases both the membrane cost and the electricity cost due to the associated increase in pressure drop.

When comparing the CL configuration to the SF configuration, increasing the number of stages results in a smaller relative reduction in membrane area. In the CL configuration, only one additional stage beyond the minimum required number of stages (to achieve a certain recovery) is required to achieve the minimum total membrane area and treatment cost. Increasing the number of stages beyond the optimum number (minimum number of stages plus one) has no effect on the total required membrane but increases the treatment cost because each additional stage of CL configuration adds an independent stream loop with a flowrate roughly equivalent to the plant makeup feed (Figure 4a), which will be discussed further in the following section. As a result, the additional membrane area in any additional stage beyond the optimum number of stages balances the membrane area reduction (due to lower terminal concentration difference) of each stage. In addition, the treatment cost increases as more power is required to pressurize and circulate the flow in the added stage.

In the case of BR configuration, there is no requirement for stage-wise salinity increase to achieve the desired recovery. In fact, a train of OARO stages in BR configuration can be thought of as a single long OARO stage with the same total area. As a result, the membrane area remains roughly constant. In summary, the total membrane area for BR, SF, and CL systems is 85.4, 86.3, and 101.9 thousand square meters, respectively, demonstrating the superiority of the BR configuration over the other two configurations when taking into account the design simplicity.

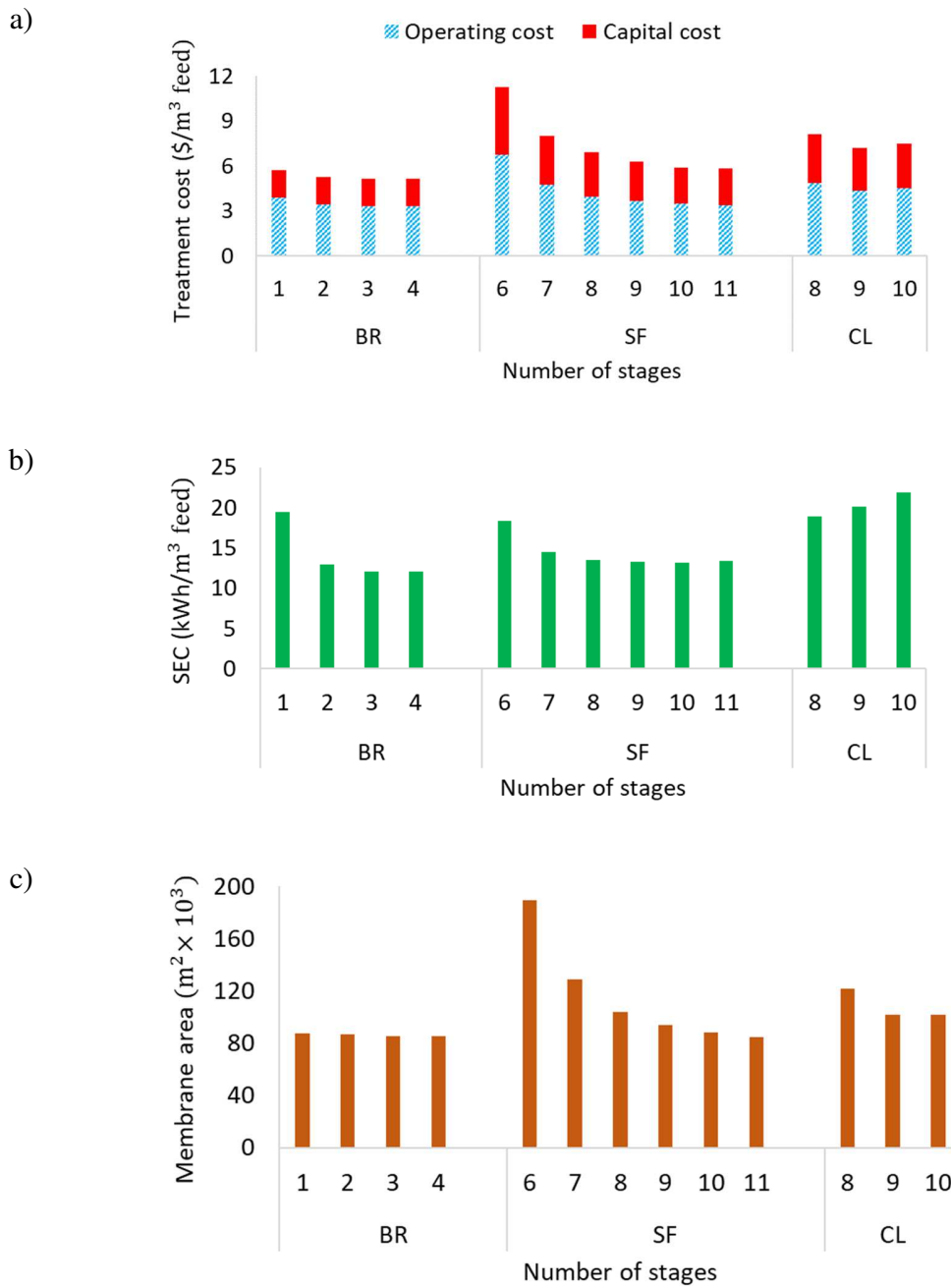


Figure 3. a) Treatment cost, b) Specific energy consumption (SEC), c) Total membrane area versus number of stages for BR, SF, and CL configurations (the stage counts exclude the initial RO stage). The feed and reject brine

salinities are fixed at 10% and 30% (wt/wt), respectively

Stage flowrate and salinity- Figures 4a and 4b illustrate the stage flowrate and salinity of the investigated OARO configurations at their cost optimum stage count. The difference between the inlet and outlet of each stage's concentrating or diluting stream (corresponding to the vertical distance between the solid and dashed lines in Figures 3a and 3b) represents the permeate production and salinity increase in that stage. The majority of permeate production and concentration increase in the BR occurs in the initial stage where salinity is lowest and flowrates are greatest while permeate production decreases in subsequent stages. Similarly, the initial stage of SF produces the greatest amount of permeate, which gradually decreases in subsequent stages. CL requires that all stages produce approximately equal amounts of permeate to maintain the system's steady state operation and satisfy the mass balance.

It is worth noting that the BR-OARO configuration achieves an appropriate balance of diluting and concentrating flowrates due to the presence of the recycle stream and the location of the feed entrance. For high salinity feed, the plant feed is added to the first OARO stage's concentrating inlet after the RO dewatering process. This compensates for permeate loss in the RO stage, and the flowrate difference (between the diluting outlet and the concentrating inlet of the first OARO stage) decreases to the volume of reject brine, which is significantly less than the volume of permeate in high recovery cases. Furthermore, if the feed salinity is low, the optimum feed entrance location is the direct entry to the RO stage inlet. As a result, the majority of permeate production (volume loss) is generated by the plant feed rather than the dilute outlet of the first OARO stage, and the difference between the concentrating inlet and the diluting outlet

of the first OARO stage is reduced. As a result, the BR-OARO configuration is well-balanced with respect to the diluting and concentrating stream flowrates. Additionally, the optimal recycle stream flowrate (dilute inlet of the final OARO stage in the BR configuration) is approximately equal to the plant feed flowrate.

For SF configuration, it is observed that the difference between the diluting and concentrating side flowrates is the greatest in the initial stages and diminishes in the final stages because the optimum split feed ratio in SF configuration varies stage-wise, being higher at the beginning and lower at the end. Reduced feed split ratio results in greater proportion of the feed flowing to the diluting side as opposed to the concentrating side. In final stages with higher salinity and lower flux, a lower split feed ratio results in less salinity reduction on the dilute side. This increases the separation driving force and alleviates the low flux of the final stages. However, in the initial stages, the split feed ratio is increased to maximize the salinity reduction of the dilute stream that enters the RO stage.

The optimum flowrates of the diluting stream outlet and concentrating stream inlet in all stages of the CL configuration are so close (and approximately equal to the plant feed flowrate) that they almost overlap. As the result, given the same permeate production in all stages, the concentrating stream outlet flowrate and diluting stream inlet flowrate in all stages are approximately equal to the final reject brine flowrate.

Stage flux and area- Figure 4c shows the area and flux of each stage for the studied OARO configurations for the cost optimal number of stages. Flux decreases stage-wise for all three configurations, with significantly higher flux occurring at the initial RO stage because the salinity of both dilute and concentrating solutions increase stagewise in all configurations (Figure 4b). Specifically, higher salinity levels are associated with higher concentration polarization,

resulting in lower flux in the final stages. The initial RO stage not only benefits from the lower salinity of the feed, but it also operates at a higher hydraulic pressure, resulting in a higher flux and smaller area than the subsequent OARO stages. In comparison to SF and BR configurations, OARO stages in CL configurations operate at a higher flux because the OARO stages in SF and BR configurations operate at higher salinities than the CL configuration in which the last OARO stage's concentrating inlet and diluting outlet salinity are bound by the plant feed salinity (Figure 4b).

Membrane area in each CL stage increases because the rate of permeate production remains constant while the flux decreases. In SF configuration, permeate production decreases stage-wise, resulting in stage-wise membrane area reduction despite the flux decrease. The initial and final OARO stages in BR configuration have the largest membrane area. This is an interesting finding and is primarily because the BR configuration consists of stages connected in series, similar to a long stage and are separated whenever the width of the stage needs to be changed in accordance with the pressure drop and Reynolds number, as described above. As such, there is no distinct trend (increasing or decreasing) in stage area of subsequent stages for the BR configuration.

Stage specific energy consumption - Figure 4d depicts the stagewise electricity consumption of the investigated configurations, as well as split of SEC attributable to the operation of the high-pressure pump, booster and low pressure pumps. For BR configuration, the majority of SEC consumption occurs in the initial RO stage and is primarily comprised of high-pressure pump SEC because the feed to each BR's OARO stage is already pressurized effluent from the preceding stage, requiring only booster and recirculation pumps to maintain the flow and separation process. The optimization results indicate that the RO outlet stream is only

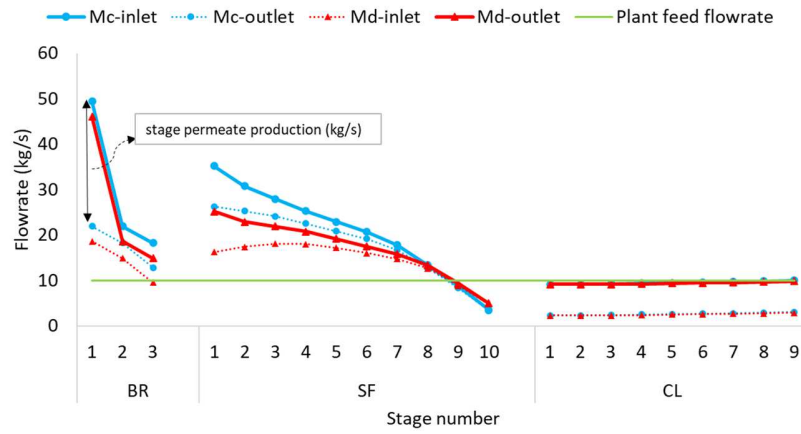
partially depressurized in the ERD device (to pressurize RO inlet stream). As a result, the RO outlet stream exits the ERD while still maintaining an elevated pressure. Additionally, this stream recovers energy from the system's reject brine prior to entering the first OARO stage via another ERD device. As a result, the concentrating stream enters the train of OARO stages without the need for additional high-pressure pumps. The first and last stage of the BR configuration have the highest SEC of recirculation/booster pumps, which is a function of the stage area and flow rate.

For SF configuration, the SEC of both the high-pressure pump and the recirculation/booster pump gradually decreases stage-by-stage proportional to the flow and membrane area of each stage. Although the concentrated effluent from each stage of the SF configuration flows to the next, each stage of the SF configuration requires a high-pressure pump to pressurize the streams because the majority of the feed stream to each SF stage comes from the subsequent stage's low-pressure diluting stream outlet, which requires pressurization. Further, the effluent from the previous stage is split between the diluting and concentrating channels, with only a portion of it going to the concentrating side. Analysis shows that for cost optimal performance of SF configuration, each stage's effluent (concentrating side outlet) must be completely depressurized before proceeding to the next stage, and its reject energy is recovered to pressurize the concentrating stream inlet for the same stage.

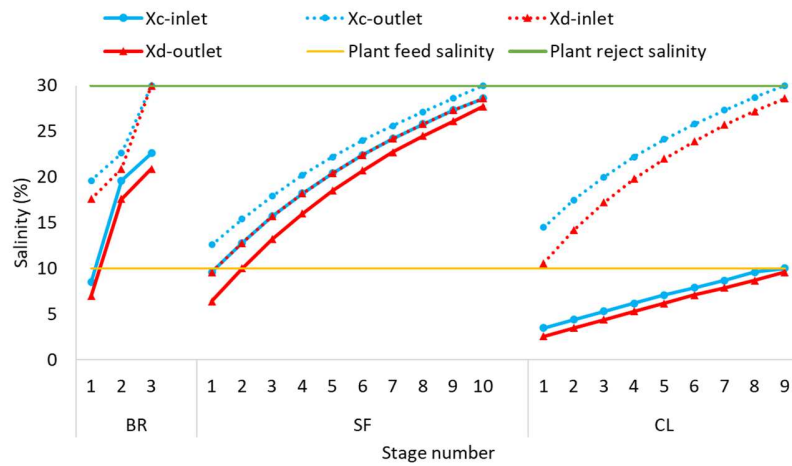
For the CL configuration, SEC of the high-pressure pump for all stages are roughly the same because they operate at the same flowrate and the effluent of each stage is completely depressurized because it serves as the dilute side inlet for the next stage. As a result, pressurization is required at each stage, and ERD devices recover energy from the reject stream

of each stage for the same stage's inlet concentrating stream. The energy required for recirculation in CL increases stage by stage as the stage area and pressure drop increase.

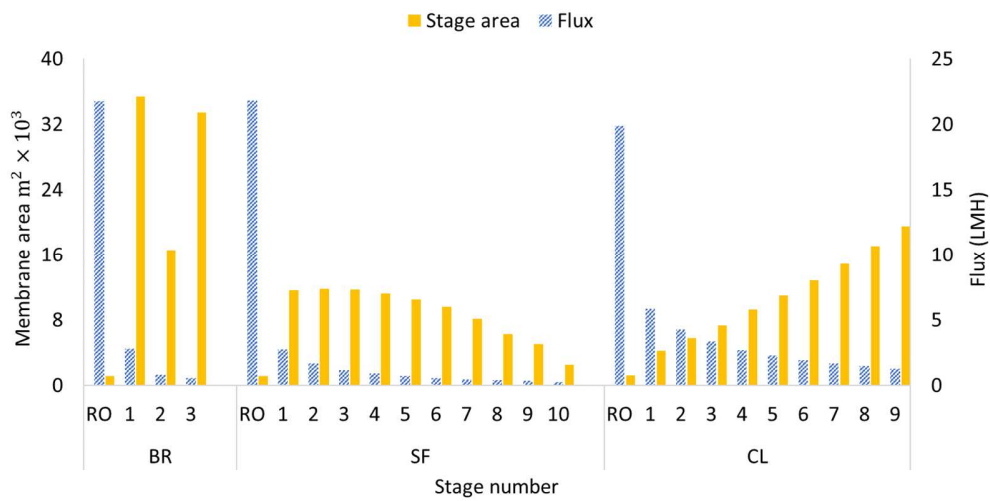
a)



b)



c)



d)

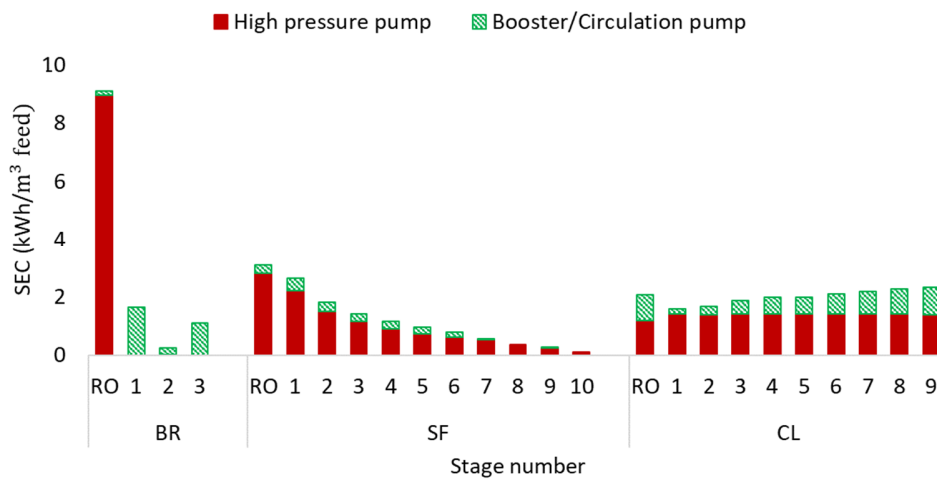


Figure 4. a) Stage flowrate, b) stage salinity, c) membrane area, d) specific energy consumption (SEC) for BR, SF, and CL configurations for cost optimal number of stages. The feed and reject brine salinities are fixed at 10% and 30% (wt/wt), respectively.

Stage applied pressure- With the exception of the RO stage in the CL configuration, all stages operate at their maximum allowable pressure in all configurations (Figure A2), which demonstrates that configuring multiple stages of OARO modules in series (for example,

COMRO and BR-OARO) does not save energy in the same way that a multi-stage RO (MSRO) system does (i.e., stagewise increase in applied pressure). This is because the large OARO membrane required has a significant impact on OARO optimum design; Lower pressure in initial stages reduces flux and increases the required membrane area of these stages, resulting in an increase in pressure drop and membrane cost. As a result, the energy savings in multiple stages of OARO module in series only occurs when changing the width and adjusting the Re of the system, as explained previously.

The applied pressure in CL's RO stage is low at the module's inlet (around 50 bar) and gradually increases to the maximum allowable level of 85 bar at the RO stage's concentrate outlet. This arrangement saves energy by operating at a lower pressure and higher flowrate at the beginning of the RO stage and a higher pressure and lower flowrate toward the RO stage's outlet. However, for BR and SF configurations, the high osmotic pressure of the RO feed inlet at high salinity (Figure 4c) prohibits the RO stage from operating at a low initial hydraulic pressure. Thus, the RO stage of the SF and BR modules operates at a maximum hydraulic applied pressure of 85 bar throughout the module's length.

Sensitivity analysis

Feed salinity- Figure 5a shows the treatment cost of three OARO configuration for two levels of feed salinity, namely 3.5% and 10%. As previously stated, feed with 3.5% salinity enters the systems at the RO inlet and feed with 10% salinity enters the systems at the RO outlet in the BR-OARO and SF-OARO configurations. The treatment costs of both SF and BR are reduced by 55 percent when the feed salinity is reduced from 10% to 3.5%, while the treatment costs of CL are only reduced by 16%. The advantage of SF and BR comes from the fact that

lowering the feed salinity results in the majority of the separation occurring in the initial RO stage. As a result, the volume of the RO effluent that requires further concentration in subsequent OARO stages decreases as does the amount of OARO permeate recirculation to the RO stage, both of which significantly reduce the treatment cost. However, in the case of CL, plant feed enters the final OARO stage via a separate loop, and permeate production is constant throughout the stages. As a result, salinity reduction has no effect on the flowrate of the OARO stages. The only reason for the slight reduction in OARO treatment cost for reduced plant inlet feed salinity is that the average salinity of all stages is reduced, which increases flux and hence membrane area requirements. This behavior is consistent with the result obtained by Chen and Yip [20], which demonstrated that the energy consumption of the CL configuration is independent of the feed salinity but is dependent on the brine salinity. As a result, the operational difference between SF and BR vs CL configuration is even more pronounced at lower salinities.

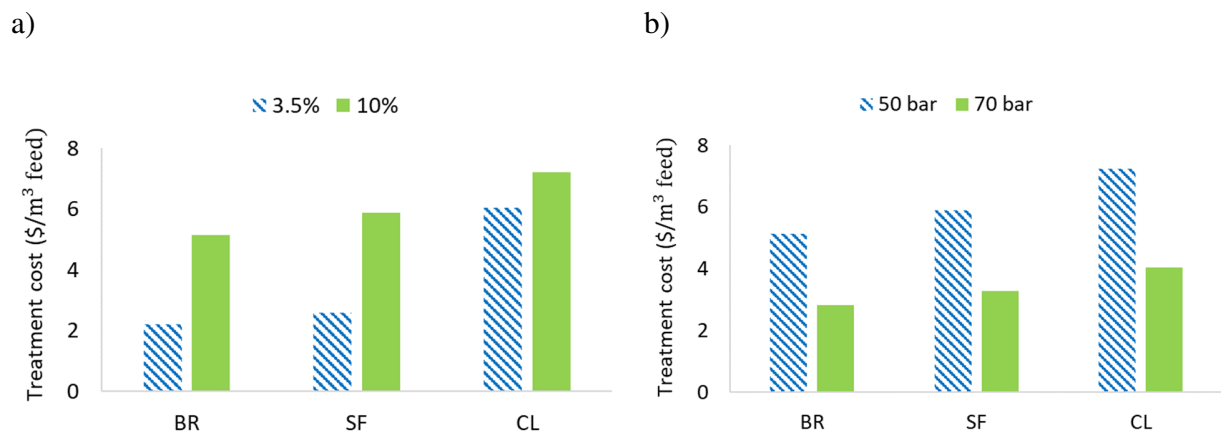


Figure 5. Cost of treatment for BR, SF, and CL configurations for: a) feed salinity of 3.5% and 10%, and b) membrane burst pressure of 50 and 70 bar for OARO membranes with plant feed salinity of 10%. Both figures show the results for a reject brine salinity of 30%.

Pressure- The effect of increasing the membrane burst pressure of OARO membranes on treatment cost is shown in Figure 5b. Increased burst pressure has roughly the same effect on all configurations in terms of relative cost savings. Increasing the burst pressure from 50 to 70 bar results in around 44 percent reduction in the cost of treatment for all configurations because higher pressure results in a greater driving force for separation, which increases flux and decreases the membrane area, resulting in a decrease in pressure drop and hence reduction in capital and operating costs.

Electricity cost, OARO membrane cost and membrane replacement rate- Appendix figures A.4 and A.5 show sensitivity analysis for cost elements (unit electricity and unit membrane cost) and membrane replacement factors for the BR-OARO configuration, which has been shown to outperform other OARO configurations. When compared to the baseline value (BV) of 0.069 \$/kWh, a 150 percent increase in electricity costs reduces the treatment cost by less than 10%. (Figure A.4a). As OARO membrane cost is the main constituent of the total treatment cost of OARO systems with large areas, a 150 percent increase in OARO membrane unit cost with a base value of 50 \$/m² significantly increases the treatment cost by 36 percent (Figure A.4b). Similarly, a 150 percent increase in membrane replacement rate, compared to a baseline of 15%, increases treatment costs by 23% (Figure A.5).

Pump efficiency: The findings of this study are presented under the assumption of a pump efficiency of 75%. Figure A.6 depicts the effect of increased pump efficiency on treatment costs and specific energy consumption for each of the three configurations. Both treatment cost and SEC decrease marginally as pump efficiency increases from 75 to 90, while the order of superiority of various configurations remains unchanged.

Conclusions

This work presented the BR-OARO configuration and developed optimization models for the BR-OARO, as well as frequently discussed CL-OARO, SF-OARO, and COMRO configurations. Each system was analyzed with two sets of single objective optimization: 1) to maximize recovery at various number of stages at two maximum OARO membrane pressure levels of 20 and 50 bar, and 2) to minimize treatment costs for a hypothetical plant concentrating 10 kg/s of hypersaline produced water with 10% salinity to reject brine with 30% salinity (corresponding to ZLD water recovery). A comparison of key performance metrics, including treatment cost, specific energy consumption, and membrane area, is presented for all configurations. The key findings from the study are summarized briefly as follows.

Regardless of the number of stages used, COMRO cannot achieve the high recoveries required for ZLD conditions at the burst pressures of 50 bar used in this study. CL and SF configurations require a large number of stages in order to achieve high recoveries. However, the single stage BR configuration can achieve ZLD recovery with a maximum applied pressure as low as 20 bar. Recovery limitation in SF and CL configurations with low stage count is primarily due to their limited dilute stream inlet salinity (not the salinity treatable by RO stage). Dilute salinity can be reduced to a level treatable by RO stage in a single stage, such as in the BR configuration.

In terms of cost, membrane area, specific energy consumption, and stage count, BR outperforms all other configurations. It is observed that the performance of the SF configuration approaches that of the BR configuration when the number of stages is increased, but at the cost of increased design complexity. Increasing the number of stages saves energy and thus lowers the cost of BR configuration, but only by about 10%. On the other hand, increasing the number

of stages in SF results in a 50 percent reduction in treatment cost due to the reduction in membrane area. The cost of the CL configuration is reduced by adding only one stage above the minimum number of stages required to achieve the desired recovery because of the savings in membrane area.

Configuring OARO stages in series results in energy savings in BR and SF, which enables the module width to be adjusted in accordance with the lower Re bound. Because of the large pressure drop in OARO stages with large areas, all configurations operate at low Re numbers. Furthermore, increasing Re number necessitates more staging in order to adjust the width and alleviate pressure drop.

The initial RO stage has the highest SEC in the BR configuration, with high pressure pump SEC being the major contributor to energy consumption, and the remaining stages only require booster and low pressure pumps. In the case of SF, the SEC of the high-pressure pumps, the booster and low pressure pumps are distributed proportionally to the membrane area and flowrate of the stages and increases stage-wise. The SEC of the CL high pressure pump is the same at all stages, while the SEC of the recirculation/booster pump increases stage by stage. The results of sensitivity analysis shows that reducing plant feed salinity (from 10% to 3.5%) lowers the treatment cost of BR and SF configurations by 56%, while it lowers the cost of the CL configuration by just 16%. Finally, increased membrane burst pressure from 50 to 70 bar reduces the treatment cost for all configurations.

Acknowledgement

This work was supported by the U.S. Department of Energy under Grant Number DE-EE0007888-10-08. Any findings expressed in this study are those of authors and do not reflect the views of the U.S. Department of Energy.

Acronyms

AF	Amortization factor
BV	Baseline value
CEPCI	chemical engineering plant cost indices
ERD	Energy recovery device

Roman symbols

A	Area	m^2
a_w	Membrane water permeability coefficient	$\frac{m^3}{h \cdot m^2 \cdot bar}$
a_s	Membrane salt permeability coefficient	$\frac{m^3}{h \cdot m^2}$
C	Concentration	$\frac{g}{L}$
C_p	Heat capacity.	$\frac{kJ}{kg \cdot K}$
D	Solute diffusion coefficient	$\frac{m^2}{h}$
d_f	Spacer filament diameter	m
d_h	Membrane channel hydraulic diameter	m
J_w	Water flux	$\frac{m^3}{h \cdot m^2}$
J_s	Salt flux	$\frac{kg}{h \cdot m^2}$
k_{mass}	Mass transfer coefficient	$\frac{m}{s}$

L	Membrane length	m
M	Mass flow rate	$\frac{\text{kg}}{\text{h}}$
m	Molality	$\frac{\text{mol}}{\text{kg}}$
OP	Osmotic pressure	bar
P	Hydraulic pressure	bar
PD	Pressure drop	$\frac{\text{bar}}{\text{m}}$
Pr	Prandtl number	
R	Universal gas constant	$\frac{\text{J}}{\text{mol. K}}$
Re	Reynolds number	
S	Size of equipment	
Sc	Schmidt number	
Sh	Sherwood number	
T	Temperature	k
V	Velocity	$\frac{\text{m}}{\text{s}}$
W	Membrane width	m
WR	Water Recovery	%
X	Salinity (weight percent)	%

Greek symbols

ρ	Density	$\frac{\text{kg}}{\text{m}^3}$
μ	Viscosity	Pa.s

ΔA	Slice area	m^2
α	Osmotic pressure coefficient	
δ	Thickness	m
η	Efficiency	%
ϵ	Porosity	%
ν	The number of dissociating ions	

subscripts

b	Bulk
c	Concentrating side
d	Diluting side
f	Make up feed
in	Inlet
l	Liquid
m	Membrane surface
out	Outlet
p	Permeate
pg	Purge
px	Pressure exchanger
rec	Recycle stream
rej	Reject stream
sp	Spacer

superscripts

i	Stage number
---	--------------

z	Slice number
firsti	First stage
firstz	First slice
lasti	Last stage
lastz	Last slice

Appendix

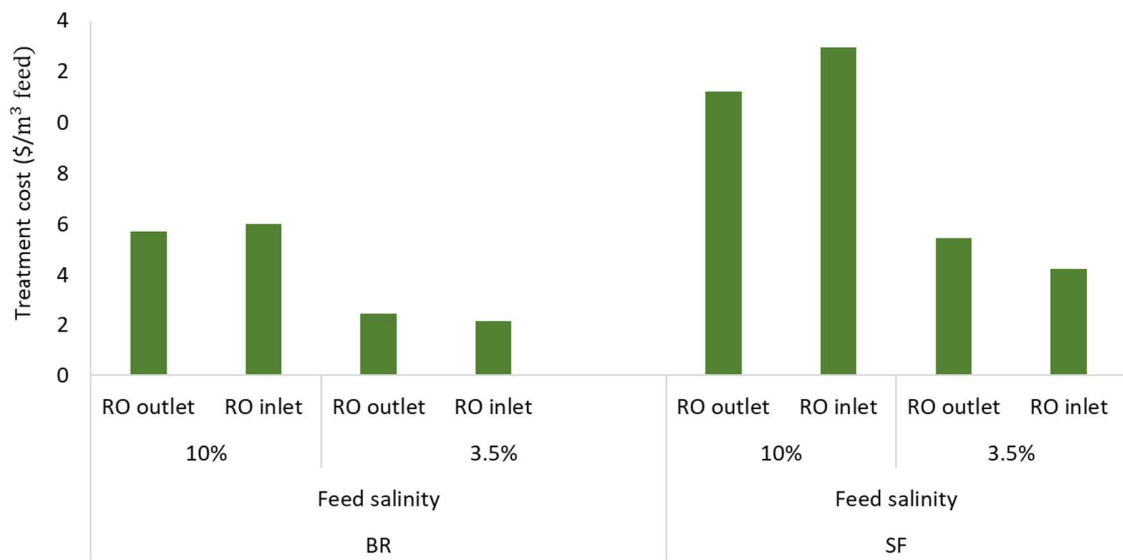


Figure A.1. Treatment cost of BR and SF configurations versus feed entrance location.

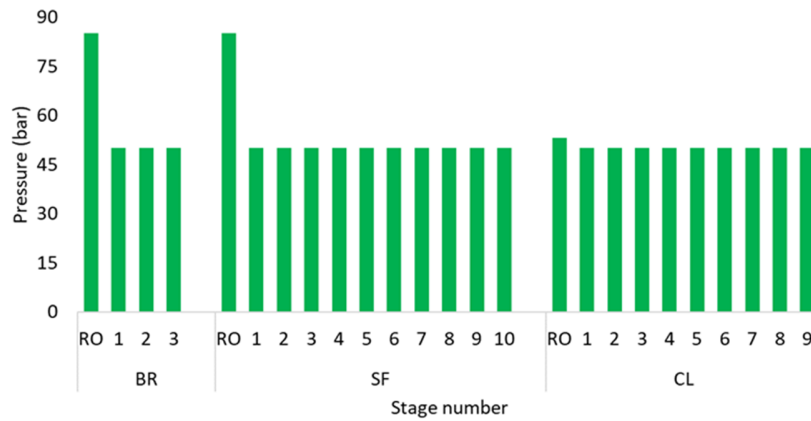


Figure A.2. Applied hydraulic pressure at concentrating inlet of each stage of BR, CL, and SF configurations.

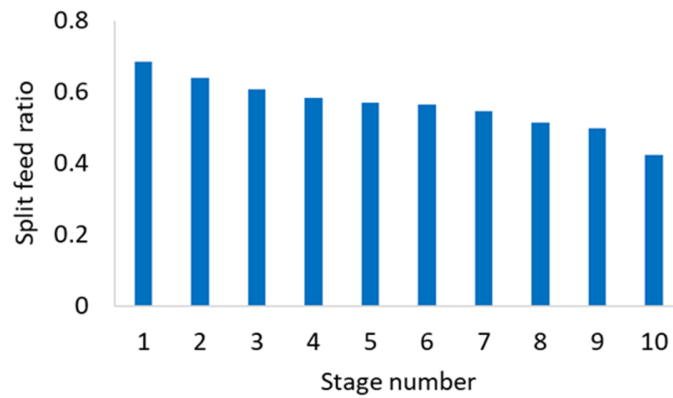


Figure A.3. Feed split ratio of each stage of SF configuration.

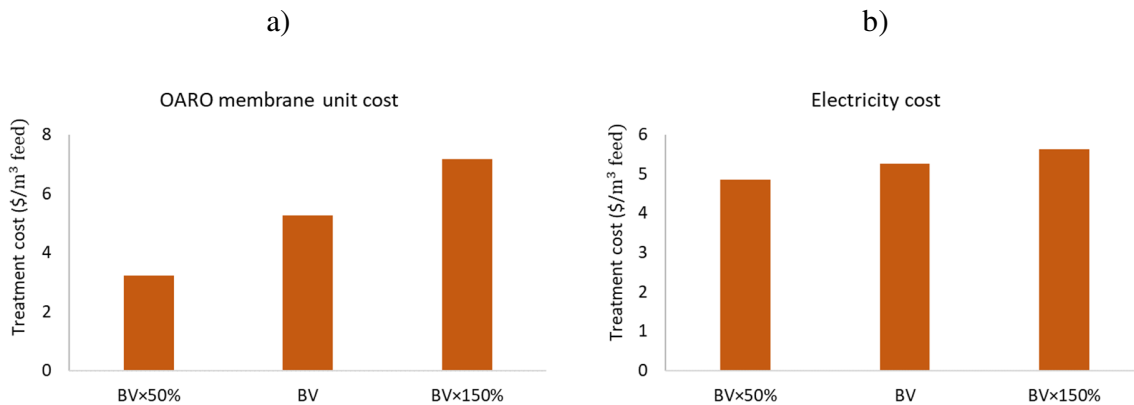


Figure A.4. Variation in minimum treatment cost of BR-OARO configuration as a function

of a) OARO membrane unit cost, and b) unit electricity cost

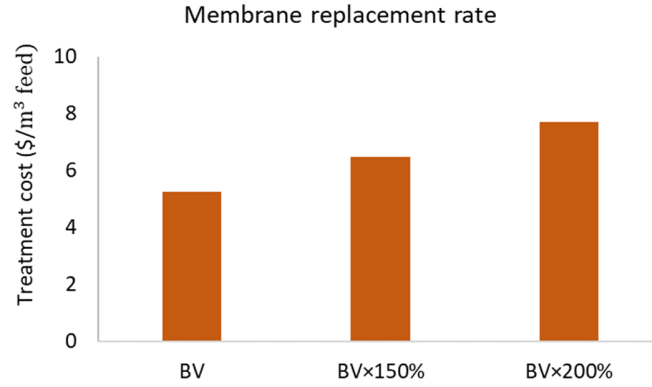


Figure A.5. Variation in minimum treatment cost of BR-OARO configuration as a function of membrane replacement rate

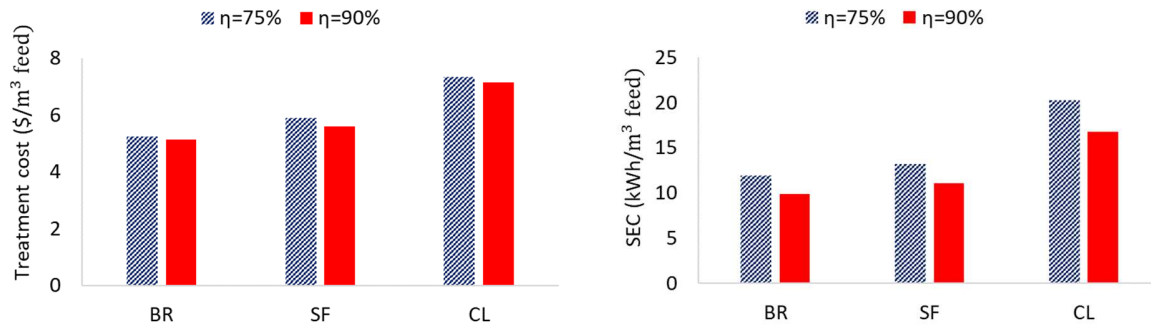


Figure A.6. Variation in minimum treatment cost and specific energy consumption of BR-OARO, SF-OARO, and CL-OARO configuration as a function of pumps efficiency

Table A.1. Operating and capital costs for a treatment plant that concentrates 10 kg/s of produced water with a salinity of 10% to reject brine with a salinity of 30%.

		BR-OARO	SF-OARO	CL- OARO
Normalized annual capital	Number of stages	3	10	9
	Membrane	1.4	1.48	1.66

costs (\$/m ³ _{feed})	High pressure pump	0.06	0.06	0.07
	Low pressure/booster pump	0.48	0.79	1.3
	Pressure exchanger	0.02	0.12	0.034
Normalized operating costs (\$/m ³ _{feed})	Electricity	0.83	0.91	1.4
	Membrane replacement	2.4	2.52	2.82
	Others (labor and chemical)	0.05	0.05	0.05

Table A.2. Plant characteristics and annual cost estimation

Produced water temperature (°C)	20
Produced water salinity (%)	10
Produced water component	NaCl
Reject brine salinity (%)	30
Plant capacity (kg/s)	10
Maximum brine salinity (%)	30
Maximum RO permeate salinity (%)	0.05
Plant life (year)	20
Interest rate (%)	5

Table A.3. Baseline values of technical parameters

		Ref
OARO membrane water permeability coefficient $\left(\frac{\text{L}}{\text{m}^2\text{h}\text{-bar}}\right)$	2.49	[36]
RO membrane water permeability coefficient $\left(\frac{\text{L}}{\text{m}^2\text{h}\text{-bar}}\right)$	1.51	[30, 38]
OARO membrane salt permeability coefficient $\left(\frac{\text{L}}{\text{m}^2\text{h}}\right)$	0.39	[36]
RO membrane salt permeability coefficient $\left(\frac{\text{L}}{\text{m}^2\text{h}}\right)$	0.12	[30, 38]
OARO membrane burst pressure (bar)	50	[36]
RO membrane burst pressure (bar)	85	[30]
OARO membrane structural parameter (μm)	564	[36]
Feed and permeate channel height (mm)	2	[30]
Channel's spacer porosity (%)	75	[30]
Pumps efficiency (%)	75	[30]
ERD efficiency (%)	90	[29]

Table A.4. Capital cost data and functions (baseline values)

Capital Cost		Size unit	Ref.
OARO Membrane	$50 \times S$	$\frac{\$}{\text{m}^2}$	[30]
RO Membrane	$30 \times S$	$\frac{\$}{\text{m}^2}$	[30, 38]
ERD	$3134.76(S)^{0.54}$	$\frac{\text{m}^3}{\text{h}}$	[30, 39]
Low pressure/booster pump	$[8000 + 240(S)^{0.9}] \times \frac{1}{3.6} \times \frac{\text{CEPCI2018}}{\text{CEPCI2010}}$	$\frac{\text{m}^3}{\text{h}}$	[40]

Table A.5. Operating cost data

Operating cost		Ref.
Electricity	$0.069 \left(\frac{\$}{\text{kwh}} \right)$	[41]
Membrane replacement	15% of initial membrane area/year	[39]
Labor and chemical cost	3 % of initial investment/year	[39]

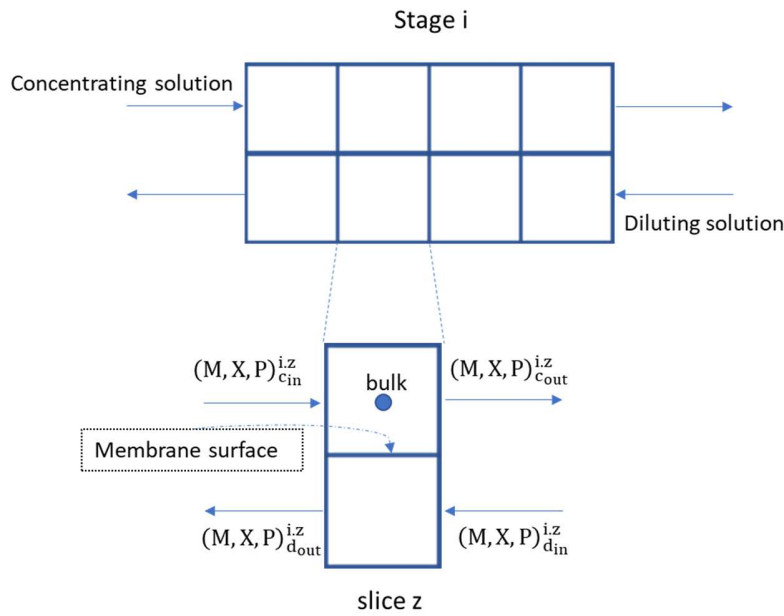


Figure A.7. Schematic of discretized RO and OARO stage modeling. The results of this study are presented for 30 slices per stage. Increasing the number of slices beyond 30 does not change the results by more than 1%.

Table A.6. Overall mass balance

	COMRO	BR-OARO	SF-OARO	CL-OARO
Total mass balance		$M_f^{\text{plant}} = M_{\text{rej}} + M_d$		$M_f^{\text{plant}} = M_{\text{rej}} + M_d + M_{\text{pg}}$
Total salt balance		$M_f^{\text{plant}} X_f^{\text{plant}} = M_{\text{rej}} X_{\text{rej}} + M_d X_d$		$M_f^{\text{plant}} X_f^{\text{plant}} = M_{\text{rej}} X_{\text{rej}} + M_d X_d + M_{\text{pg}} X_{c_{\text{out}}}^{i-1, \text{last}z}$, $i=\text{last}i$

Reject salinity and flowrate	$M_{rej} = M_{c_{out}}^{lasti,lastz}$ $X_{rej} = X_{c_{out}}^{lasti,lastz}$	$M_{rej} = M_{c_{out}}^{lasti,lastz}$ $X_{rej} = X_{c_{out}}^{lasti,lastz}$
Permeate salinity and flowrate	$M_d = M_{d_{out}}^{firsti,firstz}$ $X_d = X_{d_{out}}^{firsti,firstz}$	
Overall pure water recovery	$WR = \frac{M_d(1 - X_d)}{M_f^{plant}(1 - X_f^{plant})}$	

Table A.7. Equations of mass and energy balance between slices of one stage

Water flux	$J_w^{i,z} = a_w(P_c^{i,z} - P_d^{i,z} - OP_{c_m}^{i,z} + OP_{d_m}^{i,z})$
Salt flux	$J_s^{i,z} = a_s(C_{c_m}^{i,z} - C_{d_m}^{i,z})$
Concentrating side bulk concentration	$C_{c_b}^{i,z} = (X_{c_{in}}^{i,z} \rho_{c_{in}}^{i,z} + X_{c_{out}}^{i,z} \rho_{c_{out}}^{i,z})/2$
Diluting side bulk concentration	$C_{d_b}^{i,z} = (X_{d_{in}}^{i,z} \rho_{d_{in}}^{i,z} + X_{d_{out}}^{i,z} \rho_{d_{out}}^{i,z})/2$
Concentrating side membrane surface concentration	$C_{c_m}^{i,z} = C_{c_b}^{i,z} \exp(B^{i,z}) - \frac{J_s^{i,z}}{J_w^{i,z}} (\exp(B^{i,z}) - 1)$
Diluting side membrane surface concentration	$C_{d_m}^{i,z} = C_{d_b}^{i,z} \exp(-A^{i,z}) + \frac{J_s^{i,z}}{J_w^{i,z}} (1 - \exp(-A^{i,z}))$
Concentrating side mass balance	$M_{c_{out}}^{i,z} = M_{c_{in}}^{i,z} - (J_w^{i,z} \times \rho_w + J_s^{i,z}) L^{i,z} W^i$ $M_{c_{in}}^{i,z} = M_{c_{out}}^{i,z-1}$
Diluting side mass balance	$M_{d_{in}}^{i,z} = M_{d_{out}}^{i,z} - (J_w^{i,z} \times \rho_w + J_s^{i,z}) L^{i,z} W^i$ $M_{d_{in}}^{i,z} = M_{d_{out}}^{i,z+1}$
Concentrating side salt balance	$M_{c_{out}}^{i,z} X_{c_{out}}^{i,z} = M_{c_{in}}^{i,z} X_{c_{in}}^{i,z} - J_s^{i,z} L^{i,z} W^i$ $X_{c_{in}}^{i,z} = X_{c_{out}}^{i,z-1}$
Diluting side salt balance	$M_{d_{in}}^{i,z} X_{d_{in}}^{i,z} = M_{d_{out}}^{i,z} X_{d_{out}}^{i,z} - J_s^{i,z} L^{i,z} W^i$ $X_{d_{in}}^{i,z} = X_{d_{out}}^{i,z+1}$
Concentrating side pressure change	$P_{c_{in}}^{i,z} - P_{c_{out}}^{i,z} = PD_c^{i,z} L^{i,z}$ $P_{c_{in}}^{i,z} = P_{c_{out}}^{i,z-1} + \Delta P_{bsc}^{i,z}$
Diluting side pressure change	$P_{d_{in}}^{i,z} - P_{d_{out}}^{i,z} = PD_d^{i,z} L^{i,z}$ $P_{d_{in}}^{i,z} = P_{d_{out}}^{i,z+1} + \Delta P_{LPd}^{i,z}$ $PD_d^{firsti,z} = 0$
Slice average pressure	$P_c^{i,z} = (P_{c_{in}}^{i,z} + P_{c_{out}}^{i,z})/2$ $P_d^{i,z} = (P_{d_{in}}^{i,z} + P_{d_{out}}^{i,z})/2$

Table A.8. Equations of mass and energy balance between stages

	COMRO	BR-OARO	CL-OARO	SF-OARO
Concentrating side inlet mass flow rate	$M_{c_{in}}^{i,firstz} = M_{c_{out}}^{i-1,lastz}$, $i \neq firsti$	$M_{c_{in}}^{i,firstz} = M_{c_{out}}^{i-1,lastz} + M_f^i$, $i \neq firsti$	$M_{c_{in}}^{i,firstz} = M_{d_{out}}^{i+1,firstz}$, $i \neq lasti$	$M_{c_{in}}^{i,firstz} = (M_{c_{out}}^{i-1,lastz} + M_{d_{out}}^{i+1,firstz} + M_f^i) \times SR$, $i \neq lasti, firsti$
	$M_{c_{in}}^{i,firstz} = M_{d_{out}}^{i+1,firstz}$	$M_{c_{in}}^{i,firstz} = M_{d_{out}}^{i+1,firstz} + M_f^i$, $i = firsti$	$M_{c_{in}}^{i,firstz} = M_f^{plant}$, $i = lasti$	$M_{c_{in}}^{i,firstz} = (M_{c_{out}}^{i-1,lastz} + M_f^i) \times SR$, $i = lasti$

	$i = \text{firsti}$			$M_{\text{cin}}^{\text{firstz}} = (M_{\text{dout}}^{\text{i+1,firstz}} + M_{\text{f}}^{\text{i}}) \times \text{SR}, i = \text{firsti}$
Diluting side inlet mass flow rate	$M_{\text{din}}^{\text{i,lastz}} = M_{\text{dout}}^{\text{i+1,firstz}}, i \neq \text{lasti, firsti}$	$M_{\text{din}}^{\text{i,lastz}} = M_{\text{dout}}^{\text{i+1,firstz}}, i \neq \text{lasti, firsti}$	$M_{\text{din}}^{\text{i,lastz}} = M_{\text{cout}}^{\text{i-1,lastz}} + M_{\text{rec}}^{\text{i-1}} - M_{\text{rec}}^{\text{i}}, i \neq \text{lasti}, i > 2$	$M_{\text{din}}^{\text{i,lastz}} = (M_{\text{cout}}^{\text{i-1,lastz}} + M_{\text{dout}}^{\text{i+1,firstz}} + M_{\text{f}}^{\text{i}}) \times (1 - \text{SR}), i \neq \text{lasti, firsti}$
	$M_{\text{din}}^{\text{i,lastz}} = M_{\text{f}}^{\text{plant}}, i = \text{lasti}$	$M_{\text{din}}^{\text{i,lastz}} = M_{\text{rec}}, i = \text{lasti}$	$M_{\text{din}}^{\text{i,lastz}} = M_{\text{cout}}^{\text{i-1,lastz}} + M_{\text{rec}}^{\text{i-1}} - M_{\text{pg}}, i = \text{lasti}$	$M_{\text{din}}^{\text{firstz}} = (M_{\text{cout}}^{\text{i-1,lastz}} + M_{\text{f}}^{\text{i}}) \times (1 - \text{SR}), i = \text{lasti}$
			$M_{\text{din}}^{\text{i,lastz}} = M_{\text{cout}}^{\text{i-1,lastz}} - M_{\text{rec}}^{\text{i}}, i = 2$	
Concentrating side inlet salinity	$X_{\text{cin}}^{\text{i,firstz}} = X_{\text{cout}}^{\text{i-1,lastz}}, i \neq \text{firsti}$	$M_{\text{cin}}^{\text{i,firstz}} X_{\text{cin}}^{\text{i,firstz}} = M_{\text{cout}}^{\text{i-1,lastz}} X_{\text{cout}}^{\text{i-1,lastz}} + M_{\text{f}}^{\text{i}} X_{\text{f}}^{\text{plant}}, i \neq \text{firsti}$	$X_{\text{cin}}^{\text{i,firstz}} = X_{\text{dout}}^{\text{i+1,firstz}}, i \neq \text{lasti}$	$M_{\text{cin}}^{\text{i,firstz}} X_{\text{cin}}^{\text{i,firstz}} = (M_{\text{cout}}^{\text{i-1,lastz}} X_{\text{cout}}^{\text{i-1,lastz}} + M_{\text{dout}}^{\text{i+1,firstz}} X_{\text{dout}}^{\text{i+1,firstz}} + M_{\text{f}}^{\text{i}} X_{\text{f}}^{\text{plant}}) \times \text{SR}, i \neq \text{lasti, firsti}$
	$X_{\text{cin}}^{\text{i,firstz}} = X_{\text{dout}}^{\text{i+1,firstz}}, i = \text{firsti}$	$M_{\text{cin}}^{\text{i,firstz}} X_{\text{cin}}^{\text{i,firstz}} = M_{\text{dout}}^{\text{i+1,firstz}} X_{\text{dout}}^{\text{i+1,firstz}} + M_{\text{f}}^{\text{i}} X_{\text{f}}^{\text{plant}}, i = \text{firsti}$	$X_{\text{cin}}^{\text{i,firstz}} = X_{\text{f}}^{\text{plant}}, i = \text{lasti}$	$M_{\text{cin}}^{\text{i,firstz}} X_{\text{cin}}^{\text{i,firstz}} = (M_{\text{cout}}^{\text{i-1,lastz}} X_{\text{cout}}^{\text{i-1,lastz}} + M_{\text{f}}^{\text{i}} X_{\text{f}}^{\text{plant}}) \times \text{SR}, i = \text{lasti}$
				$M_{\text{cin}}^{\text{i,firstz}} X_{\text{cin}}^{\text{i,firstz}} = (M_{\text{dout}}^{\text{i+1,firstz}} X_{\text{dout}}^{\text{i+1,firstz}} + M_{\text{f}}^{\text{i}} X_{\text{f}}^{\text{plant}}) \times \text{SR}, i = \text{firsti}$
Diluting side inlet salinity	$X_{\text{din}}^{\text{i,lastz}} = X_{\text{dout}}^{\text{i+1,firstz}}, i \neq \text{lasti, firsti}$	$X_{\text{din}}^{\text{i,lastz}} = X_{\text{dout}}^{\text{i+1,firstz}}, i \neq \text{lasti, firsti}$	$M_{\text{din}}^{\text{i,lastz}} X_{\text{din}}^{\text{i,lastz}} = M_{\text{cout}}^{\text{i-1,lastz}} X_{\text{cout}}^{\text{i-1,lastz}} + M_{\text{rec}}^{\text{i-1}} X_{\text{cout}}^{\text{i-2,lastz}} - M_{\text{rec}}^{\text{i}} X_{\text{cout}}^{\text{i-1,lastz}}, i \neq \text{lasti}, i > 2$	$M_{\text{din}}^{\text{i,lastz}} X_{\text{din}}^{\text{i,lastz}} = (M_{\text{cout}}^{\text{i-1,lastz}} X_{\text{cout}}^{\text{i-1,lastz}} + M_{\text{dout}}^{\text{i+1,firstz}} X_{\text{dout}}^{\text{i+1,firstz}} + M_{\text{f}}^{\text{i}} X_{\text{f}}^{\text{plant}}) \times (1 - \text{SR}), i \neq \text{lasti, firsti}$
	$X_{\text{din}}^{\text{i,lastz}} = X_{\text{f}}^{\text{plant}}, i = \text{lasti}$	$X_{\text{din}}^{\text{i,lastz}} = X_{\text{rej}}, i = \text{lasti}$	$M_{\text{din}}^{\text{i,lastz}} X_{\text{din}}^{\text{i,lastz}} = M_{\text{cout}}^{\text{i-1,lastz}} X_{\text{cout}}^{\text{i-1,lastz}} + M_{\text{rec}}^{\text{i-1}} X_{\text{cout}}^{\text{i-2,lastz}} - M_{\text{pg}} X_{\text{cout}}^{\text{i-1,lastz}}, i = \text{lasti}$	$M_{\text{din}}^{\text{i,firstz}} X_{\text{din}}^{\text{i,firstz}} = (M_{\text{cout}}^{\text{i-1,lastz}} X_{\text{cout}}^{\text{i-1,lastz}} + M_{\text{f}}^{\text{i}} X_{\text{f}}^{\text{plant}}) \times (1 - \text{SR}), i = \text{lasti}$
			$M_{\text{din}}^{\text{i,lastz}} X_{\text{din}}^{\text{i,lastz}} = M_{\text{cout}}^{\text{i-1,lastz}} X_{\text{cout}}^{\text{i-1,lastz}} - M_{\text{rec}}^{\text{i}} X_{\text{cout}}^{\text{i-1,lastz}}, i = 2$	
Feed inlet	-	$M_{\text{f}}^{\text{i}} = M_{\text{f}}^{\text{plant}}, i = \text{feed inlet}$ $M_{\text{f}}^{\text{i}} = 0, i \neq \text{feed inlet}$	-	$M_{\text{f}}^{\text{i}} = M_{\text{f}}^{\text{plant}}, i = \text{feed inlet}$ $M_{\text{f}}^{\text{i}} = 0, i \neq \text{feed inlet}$
Concentrating side stage inlet pressure	$P_{\text{cin}}^{\text{i,firstz}} = P_{\text{cout}}^{\text{i-1,lastz}} - \Delta P_{\text{ERD}}^{\text{i-1}} + \Delta P_{\text{HP+ERD}}^{\text{i}}, i = 2$	$P_{\text{cin}}^{\text{i,firstz}} = P_{\text{cout}}^{\text{i-1,lastz}} - \Delta P_{\text{ERD}}^{\text{i-1}} + \Delta P_{\text{HP}}^{\text{i}}, i = 2$	$P_{\text{cin}}^{\text{i,firstz}} = 1 + \Delta P_{\text{HP+ERD}}^{\text{i}}$	$P_{\text{cin}}^{\text{i,firstz}} = 1 + \Delta P_{\text{HP+ERD}}^{\text{i}}$

	$P_{Cin}^{i,firstz} = P_{Cout}^{i-1,lastz} - \Delta P_{ERD}^{i-1} + \Delta P_{HP+ERD}^i, \quad i \neq 2$	$P_{Cin}^{i,firstz} = P_{Cout}^{i-1,lastz} - \Delta P_{ERD}^{i-1} + \Delta P_{HP}^i, \quad i \neq 2$		
Diluting side stage inlet pressure	$P_{din}^{i,lastz} = P_{Cout}^{i+1,firstz} + \Delta P_{LPd}^{i,lastz}, \quad i \neq lasti$	$P_{din}^{i,lastz} = P_{Cout}^{i+1,firstz} + \Delta P_{LPd}^{i,lastz}, \quad i \neq lasti$	$P_{din}^{i,lastz} = 1 + \Delta P_{LPd}^{i,lastz}$	$P_{din}^{i,lastz} = 1 + \Delta P_{LPd}^{i,lastz}$
	$P_{din}^{i,lastz} = 1 + \Delta P_{LPd}^{i,lastz}, \quad i = lasti$	$P_{din}^{i,lastz} = 1 + \Delta P_{LPd}^{i,lastz}, \quad i = lasti$		

*Inlet salinity and flowrate of the dilute/permeate side of the initial RO stage is set to zero for all configurations

High pressure pumps are assumed to be located prior to the concentrating side of each stage. For the purposes of analysis, we assume low pressure and booster pumps are located between each two slices of a membrane stage (i.e. the intersection of slices overlap with intersection of modules in series with customized lengths). The optimization process will determine whether the pumps are active and supplying energy. The capital cost formulation in the model is such that if a pump does not provide energy, no capital cost for that pump is accounted for. The capital cost of booster and low pressure pumps will prevent a large number of these pumps from being installed.

Table A.9. Power consumption calculation

	COMRO	BR-OARO	CL-OARO	SF-OARO
Stage total HP pump power consumption	$TP_{HP}^i = \left(\frac{M_{cin}^{i,firstz} \Delta P_{HP+ERD}^i}{\rho_{cin}^{i,firstz}} - \frac{M_{cout}^{i,lastz} (P_{Cout}^{i,lastz} - 1) \eta_{px}}{\rho_{cout}^{i,lastz}} \right) \frac{1}{36 \eta_p}, \quad i = firsti$		$TP_{HP}^i = \left(\frac{M_{cin}^{i,firstz} \Delta P_{HP+ERD}^i}{\rho_{cin}^{i,firstz}} - \frac{M_{cout}^{i,lastz} (P_{Cout}^{i,lastz} - 1) \eta_{px}}{\rho_{cout}^{i,lastz}} \right) \frac{1}{36 \eta_p}$	
	$TP_{HP}^i = \left(\frac{M_{cin}^{i,firstz} \Delta P_{HP+ERD}^i}{\rho_{cin}^{i,firstz}} - \frac{M_{cout}^{lasti,lastz} (P_{Cout}^{lasti,lastz} - 1) \eta_{px}}{\rho_{cout}^{lasti,lastz}} \right) \frac{1}{36 \eta_p}, \quad i = 2$			

	$TP_{HP}^i = \left(\frac{M_{c_{in}}^{i,firstz} \Delta P_{HP+ERD}^i}{\rho_{c_{in}}^{i,firstz}} \right) \frac{1}{36 \eta_p},$ $i > 2$	
Stage total LP/booster pump power consumption	$TP_{LP/bs}^i = \sum_z \frac{M_{c/d_{in}}^{i,z} \Delta P_{LPd}^{i,z}}{36 \rho_{d_{in}}^{i,z} \eta_p}$	
Total unit power consumption	$TUP = \frac{\rho_f^{plant}}{M_f^{plant}} \sum_i (TP_{HP}^i + TP_{LP/bs}^i)$	

Table A.10. Correlations

Brine viscosity	$\mu = 2.239 \times 10^{-4} m^{0.2306}$	[42]
Brine density	$\rho = 1028.58 + 38.23m - 1.043m^2$	[42]
Osmotic pressure	$OP = \frac{iRT}{M_w} C(3.33 \times 10^{-6} C^2 + 1.78 \times 10^{-4} C + 0.918)$	[30]
Hydraulic diameter	$d_h = \frac{4\epsilon d_f \delta_{sp}}{(2d_f + 4(1 - \epsilon)\delta_{sp})}$	[43]
Velocity	$V = \frac{M_{in}}{(W_m \delta_{sp} \epsilon \rho)}$	
Reynolds number	$Re = \frac{\rho V d_h}{\mu}$	
Prandtl's number	$Pr = \frac{\mu C_p}{k}$	
Schmidt number	$Sc = \frac{\mu}{\rho \cdot D}$	
Sherwood number	$Sh = 0.2Re^{0.57} Sc^{0.4}$	[44]
Mass transfer coefficient	$k_{mass} = \frac{D \cdot Sh}{d_h}$	
Pressure drop	$PD = \left(0.42 + \frac{189.3}{Re} \right) \frac{\rho V^2}{2d_h}$	[45]
CP coefficient-diluting side	$A^{i,z} = J_w^{i,z} \times \left(\frac{S}{D} + \frac{1}{k_{mass d}} \right)$	[30]

CP coefficient-
concentrating side

$$B^{i,z} = \frac{J_w^{i,z}}{k_{\text{mass}_c}}$$

[30]

References

1. Butkovskiy, A., et al., *Organic pollutants in shale gas flowback and produced waters: identification, potential ecological impact, and implications for treatment strategies*. Environmental science & technology, 2017. **51**(9): p. 4740-4754.
2. Pichtel, J., *Oil and gas production wastewater: Soil contamination and pollution prevention*. Applied and Environmental Soil Science, 2016. **2016**.
3. Gregory, K.B., R.D. Vidic, and D.A. Dzombak, *Water management challenges associated with the production of shale gas by hydraulic fracturing*. Elements, 2011. **7**(3): p. 181-186.
4. Brantley, S.L., et al., *Water resource impacts during unconventional shale gas development: The Pennsylvania experience*. International Journal of Coal Geology, 2014. **126**: p. 140-156.
5. Conidi, C., et al., *Treatment of flue gas desulfurization wastewater by an integrated membrane-based process for approaching zero liquid discharge*. Membranes, 2018. **8**(4): p. 117.
6. Wales, M.D., et al., *Flue Gas Desulfurization (FGD) Wastewater Treatment Using Polybenzimidazole (PBI) Hollow Fiber (HF) Membranes*. Membranes, 2021. **11**(6): p. 430.
7. Mohamed, A., M. Maraqa, and J. Al Handhaly, *Impact of land disposal of reject brine from desalination plants on soil and groundwater*. Desalination, 2005. **182**(1-3): p. 411-433.
8. Panagopoulos, A. and K.-J. Haralambous, *Environmental impacts of desalination and brine treatment-Challenges and mitigation measures*. Marine Pollution Bulletin, 2020. **161**: p. 111773.
9. Tong, T. and M. Elimelech, *The global rise of zero liquid discharge for wastewater management: drivers, technologies, and future directions*. Environmental science & technology, 2016. **50**(13): p. 6846-6855.
10. Yaqub, M. and W. Lee, *Zero-liquid discharge (ZLD) technology for resource recovery from wastewater: A review*. Science of the total environment, 2019. **681**: p. 551-563.
11. Angelini, P., et al., *Materials for separation technologies: Energy and emission reduction opportunities*. DOE, EERE Office, Washington, DC, 2005. **103**.
12. Shao, L., *Grand Challenges in Emerging Separation Technologies*. Frontiers in Environmental Chemistry, 2020. **1**: p. 3.
13. Vane, L., *Separations Versus Sustainability: There Is No Such Thing As a Free Lunch, in Sustainability in the Design, Synthesis and Analysis of Chemical Engineering Processes*. 2016, Elsevier. p. 35-65.
14. Jones, E., et al., *The state of desalination and brine production: A global outlook*. Science of the Total Environment, 2019. **657**: p. 1343-1356.
15. Ahunbay, M.G., S.B. Tantekin-Ersolmaz, and W.B. Krantz, *Energy optimization of a multistage reverse osmosis process for seawater desalination*. Desalination, 2018. **429**: p. 1-11.
16. Zhu, A., P.D. Christofides, and Y. Cohen, *Effect of thermodynamic restriction on energy cost optimization of RO membrane water desalination*. Industrial & Engineering Chemistry Research, 2008. **48**(13): p. 6010-6021.
17. El-Halwagi, M.M., *Synthesis of reverse-osmosis networks for waste reduction*. AIChE Journal, 1992. **38**(8): p. 1185-1198.
18. Lin, S. and M. Elimelech, *Staged reverse osmosis operation: Configurations, energy efficiency, and application potential*. Desalination, 2015. **366**: p. 9-14.

19. Mistry, K.H., et al., *Entropy generation analysis of desalination technologies*. Entropy, 2011. **13**(10): p. 1829-1864.
20. Chen, X. and N.Y. Yip, *Unlocking high-salinity desalination with cascading osmotically mediated reverse osmosis: Energy and operating pressure analysis*. Environmental science & technology, 2018. **52**(4): p. 2242-2250.
21. Kim, J., et al., *Osmotically enhanced dewatering-reverse osmosis (OED-RO) hybrid system: Implications for shale gas produced water treatment*. Journal of Membrane Science, 2018. **554**: p. 282-290.
22. Atia, A.A., N.Y. Yip, and V. Fthenakis, *Pathways for minimal and zero liquid discharge with enhanced reverse osmosis technologies: Module-scale modeling and techno-economic assessment*. Desalination, 2021. **509**: p. 115069.
23. Park, K. and D.R. Yang, *Cost-based feasibility study and sensitivity analysis of a new draw solution assisted reverse osmosis (DSARO) process for seawater desalination*. Desalination, 2017. **422**: p. 182-193.
24. Kim, J., D.I. Kim, and S. Hong, *Analysis of an osmotically-enhanced dewatering process for the treatment of highly saline (waste) waters*. Journal of Membrane Science, 2018. **548**: p. 685-693.
25. Peters, C.D. and N.P. Hankins, *Osmotically assisted reverse osmosis (OARO): Five approaches to dewatering saline brines using pressure-driven membrane processes*. Desalination, 2019. **458**: p. 1-13.
26. Thiel, G.P., R.K. McGovern, and S.M. Zubair, *Thermodynamic equipartition for increased second law efficiency*. Applied energy, 2014. **118**: p. 292-299.
27. Bouma, A.T., *Split-feed counterflow reverse osmosis for brine concentration*. Desalination, 2018. **445**: p. 280-291.
28. Loeb, S. and M. Bloch, *Countercurrent flow osmotic processes for the production of solutions having a high osmotic pressure*. Desalination, 1973. **13**(2): p. 207-215.
29. Bartholomew, T.V., et al., *Osmotically assisted reverse osmosis for high salinity brine treatment*. Desalination, 2017. **421**: p. 3-11.
30. Bartholomew, T.V., N.S. Siefert, and M.S. Mauter, *Cost optimization of osmotically assisted reverse osmosis*. Environmental science & technology, 2018. **52**(20): p. 11813-11821.
31. Peters, C.D. and N.P. Hankins, *The synergy between osmotically assisted reverse osmosis (OARO) and the use of thermo-responsive draw solutions for energy efficient, zero-liquid discharge desalination*. Desalination, 2020. **493**: p. 114630.
32. Zhang, S. and T.-S. Chung, *Minimizing the instant and accumulative effects of salt permeability to sustain ultrahigh osmotic power density*. Environmental science & technology, 2013. **47**(17): p. 10085-10092.
33. Chou, S., R. Wang, and A.G. Fane, *Robust and high performance hollow fiber membranes for energy harvesting from salinity gradients by pressure retarded osmosis*. Journal of membrane science, 2013. **448**: p. 44-54.
34. Kim, Y.C. and M. Elimelech, *Adverse impact of feed channel spacers on the performance of pressure retarded osmosis*. Environmental science & technology, 2012. **46**(8): p. 4673-4681.
35. Song, X., Z. Liu, and D.D. Sun, *Energy recovery from concentrated seawater brine by thin-film nanofiber composite pressure retarded osmosis membranes with high power density*. Energy & Environmental Science, 2013. **6**(4): p. 1199-1210.
36. Straub, A.P., N.Y. Yip, and M. Elimelech, *Raising the bar: Increased hydraulic pressure allows unprecedented high power densities in pressure-retarded osmosis*. Environmental Science & Technology Letters, 2014. **1**(1): p. 55-59.
37. Drud, A.S., *CONOPT—a large-scale GRG code*. ORSA Journal on computing, 1994. **6**(2): p. 207-216.

38. Lu, Y.-Y., et al., *Optimum design of reverse osmosis system under different feed concentration and product specification*. Journal of membrane science, 2007. **287**(2): p. 219-229.
39. Park, C., et al., *Stochastic cost estimation approach for full-scale reverse osmosis desalination plants*. Journal of Membrane Science, 2010. **364**(1-2): p. 52-64.
40. Hitsov, I., et al., *Economic modelling and model-based process optimization of membrane distillation*. Desalination, 2018. **436**: p. 125-143.
41. Tavakkoli, S., et al., *A techno-economic assessment of membrane distillation for treatment of Marcellus shale produced water*. Desalination, 2017. **416**: p. 24-34.
42. Swaminathan, J., *Design and operation of membrane distillation with feed recirculation for high recovery brine concentration*. Desalination, 2018. **445**: p. 51-62.
43. Da Costa, A., A. Fane, and D. Wiley, *Spacer characterization and pressure drop modelling in spacer-filled channels for ultrafiltration*. Journal of membrane science, 1994. **87**(1-2): p. 79-98.
44. Koutsou, C.P., S.G. Yiantsios, and A.J. Karabelas, *A numerical and experimental study of mass transfer in spacer-filled channels: Effects of spacer geometrical characteristics and Schmidt number*. Journal of Membrane Science, 2009. **326**(1): p. 234-251.
45. Guillen, G. and E.M. Hoek, *Modeling the impacts of feed spacer geometry on reverse osmosis and nanofiltration processes*. Chemical Engineering Journal, 2009. **149**(1-3): p. 221-231.